electronics

Article

Control of Photovoltaic Plants Interconnected via VSC to Improve Power Oscillations in a Power System

Ángeles Medina-Quesada [1,*], Walter Gil-González [2], Oscar Danilo Montoya [3,4,*], Alexander Molina-Cabrera [5] and Jesus C. Hernández [1]

1 Department of Electrical Engineering, University of Jaén, Campus Lagunillas s/n, Edificio A3, 23071 Jaén, Spain; jcasa@ujaen.es
2 Facultad de Ingeniería, Institución Universitaria Pascual Bravo, Medellín 050034, Colombia; walter.gil@pascualbravo.edu.co
3 Grupo de Compatibilidad e Interferencia Electromagnética, Facultad de Ingeniería, Universidad Distrital Francisco José de Caldas, Bogotá 110231, Colombia
4 Laboratorio Inteligente de Energía, Facultad de Ingeniería, Universidad Tecnológica de Bolívar, Cartagena 131001, Colombia
5 Grupo de Investigación en Campos Electromagnéticos y Fenómenos Energéticos, Facultad de Ingeniería, Universidad Tecnológica de Pereira, Pereira 660003, Colombia; almo@utp.edu.co
* Correspondence: aquesada@ujaen.es (Á.M.-Q.); odmontoyag@udistrital.edu.co (O.D.M.)

Abstract: This paper presents an integrated methodology applied to photovoltaic (PV) plants for improving the dynamic performance of electric power systems. The proposed methodology is based on primary frequency control, which adds an ancillary signal to the voltage reference of the DC-link for the voltage source converter (VSC) in order to reduce power oscillations. This ancillary signal is computed by relating the energy stored in the VSC of the DC-link and the energy stored in the synchronous machine's shaft. In addition, the methodology considers the operating limits of the VSC, which prioritizes active power over reactive power. Furthermore, the VSC control is assessed with interconnection and damping assignment passivity-based control (IDA-PBC), as well as compared to conventional PI control. IDA-PBC is employed to design a Lyapunov asymptotically stable controller using the Hamiltonian structural properties of the open-loop model of the VSC. A 12-bus test system that considers PV plants is employed to compare the proposed IDA-PBC control with a classical proportional-integral control approach. The impact of the proposed methodology is analyzed in four scenarios with different PV penetration levels (10%, 30%, 50%, and 80%) and four large disturbances in the test power system. In addition, a decrease in the inertia of the synchronous machines from 100 to 25% is analyzed. The time-domain simulation results show that the frequency oscillations are reduced by 16.8%, 38.43%, 37.53%, and 76.94% in comparison with the case where the proposed methodology was not implemented. The simulations were conducted using the SimPowerSystems toolbox of the MATLAB/Simulink software.

Keywords: power oscillation; primary frequency control; photovoltaic plants; inertia reduction

check for updates

Citation: Medina-Quesada, Á.; Gil-González, W.; Montoya, O.D.; Molina-Cabrera, A.; Hernández, J.C. Control of Photovoltaic Plants Interconnected via VSC to Improve Power Oscillations in a Power System. *Electronics* **2022**, *11*, 1744. https://doi.org/10.3390/electronics11111744

Academic Editor: Kai Fu

Received: 22 April 2022
Accepted: 29 May 2022
Published: 31 May 2022

Publisher's Note: MDPI stays neutral with regard to jurisdictional claims in published maps and institutional affiliations.

Copyright: © 2022 by the authors. Licensee MDPI, Basel, Switzerland. This article is an open access article distributed under the terms and conditions of the Creative Commons Attribution (CC BY) license (https://creativecommons.org/licenses/by/4.0/).

1. Introduction

Power systems have evolved from conventional power grids based on traditional generation technologies that included hydraulic and thermal (coal- and natural gas-burning power plants, etc.) generation to systems with high degrees of penetration of distributed energy resources (DERs) [1]. The main types of DERs are wind power and solar photovoltaic (PV) generation. This transformation in the structure of power grids is mainly due to the growing global concern with regard to the hazardous effects of global warming, as evidenced by the agreement on climate change signed in Paris in 2015 [2]. The purpose of the agreement is to reduce the greenhouse effects caused by the many millions of tons of contaminant gases emitted into the atmosphere mainly by electrical and transport

systems [3]. The integration of DERs into electrical systems can help reduce greenhouse gas emissions because fossil fuels can be replaced by renewable generation [4].

The main disadvantage of DER systems is the high variability of the primary energy resource (solar radiation or wind speed), in addition to modifying the analysis of the power system from their power flow patterns and their stable and dynamic state [3].

A PV plant is inherently inertia-less and can generate prolonged power oscillations during large disturbances. These oscillations have low frequencies and are characteristic of an interconnected power system. Oscillations increase when the inertia of the power system is reduced, as is the case for an energy system with high penetration of renewable energy resources [5]. In addition, these oscillations can cause the power system to black out completely, which is highly undesirable [6]. Some studies have also shown that large disturbances can generate oscillations in the load angle when PV penetration is higher than 20% [6]. In other cases, it has been determined that PV penetration induces negative damping [7].

The current literature contains few studies focused on investigating the effects of PV plants on the stability of power systems. This study addresses the enhancement of power oscillation damping (POD) in a power system without constraining the dynamics of the voltage source converter (VSC) to behave as a virtual synchronous generator. This is based on primary frequency and voltage control, and, therefore, it involves using PV plants as dynamic compensators under fault events. In addition, this study attempts to utilize the Hamiltonian open-loop structure of the VSC and its natural energy model. Thereupon, it aims to design an asymptotically stable controller based on Lyapunov's theory [8]. One of the drivers that best utilizes the dynamic structure of VSCs is the passivity-based control (PBC) approach.

Several studies have investigated the transient stability of power systems with high levels of penetration of renewable resources. In [9], the authors investigated the effect of high penetration of wind power on the dynamics of a power system and its contribution to frequency regulation. Ref. [10] conducted research on methods to compensate for the low inertia of DERs in an isolated power system based on an energy storage system. In [11], the authors analyzed the stability of the power system in Canada for different penetration levels of DERs. Ref. [12] studied the frequency stability problems in Europe, and [13] modeled wind power as a STATCOM to supply reactive power during grid faults without affecting stability. Although these approaches meet the standards of power systems, they do not focus on achieving harmonious interactions with the network.

Meanwhile, other authors have focused on DER controllers for improving the stability of power systems. For example, in [14], the authors focused on under-frequency events caused by wind power trips. They determined that the frequency excursion depth is affected by the inertial response of online generation. In [15], a methodology for improving the frequency stability of power systems with a high level of DER penetration was analyzed. In [16], the authors proposed a step-down modulation control method in order to allow large-scale solar PV plants to damp electromechanical oscillations. This method is based on active power modulation and does not require curtailment as in other approaches. In [17], a linear neural network is used to propose an adaptive control in order to reduce power oscillations in wind-integrated power systems. This control injects a supplementary control signal in the rotor-side converter of the wind turbine based on a doubly-fed induction generator. In [18], a wide-area damping control is performed to stabilize inter-area oscillations by using phasor measurement unit (PMU) data. Ref. [19] employs particle swarm optimization (PSO) to tune the power system stabilizer (PSS) parameters in order to enhance the transient stability of the power system. However, [18,19] do not consider the penetration of renewable resources in power systems. Hence, it is not possible to analyze the effect of its proposal in this scenario.

Several studies have used different types of devices to improve power oscillations in power systems. Among the most common devices are FACTS [20,21], static VAR compensators (SVCs) [22], and STATCOMs [23]. A clustering technique combined with catastrophe

theory and multi-objective particle swarm optimization was presented in [20] with the purpose of optimally placing controlled series capacitors (TCSCs). The goal of this allocation goal was to enhance the transient stability of a power system. Aiming to improve transient stability, [21] analyzed the implementation of a unified power flow controller, a static synchronous series compensator, and an SVC. In [22], an SVC was employed to stabilize the power system under transient stability events, and, [23] described combined genetic and PSO algorithms to optimize STATCOM-POD in a wind-PV-thermal-bundled power system.

Other studies, while focusing on modeling the VSC as a virtual synchronous generator, analyzed electrical distribution systems with high-level DER penetration, such as microgrids or smart grids [24–26]. The effects and impacts of DERs on a transmission power system were analyzed in [27,28]. In these studies, PV systems are modeled as virtual synchronous generators. An adaptive virtual synchronous machine for power systems based on LQR was proposed in [29]. In [30], the authors determined the most vulnerable parts of a power system while considering a high penetration of converters. DER systems were modeled as virtual synchronous generators in these studies. Nevertheless, this concept does not consider the intrinsic low inertia of these devices and is not likely to produce the desired effect on power grids.

It is important to highlight that many of the previous studies do not consider the penetration of photovoltaic energy, and those that do include it worked with levels of PV penetration of less than 50%. Furthermore, these investigations do not analyze the decrease in the inertia of synchronous machines and its effect on the stability of power systems.

This study proposes a methodology for improving the POD in a power system with high levels of PV penetration. This methodology consists of injecting inertia into the power system through the PV plants, which is why the concepts of primary frequency and voltage control are implemented. These controls do not force the VSC in PV plants to behave as a virtual synchronous generator. The proposed methodology works together with primary frequency control, where an auxiliary signal is added to the reference voltage of the DC-link of the VSC to damp power oscillations. This methodology was developed by equating the energy stored in the capacitor and stored in the synchronous machines' shaft. In addition, the methodology takes into account the operating limits of the VSC, so the active power is considered before the reactive power. It also includes a dead-band in the primary frequency control to filter the noise in the frequency signal in order to reduce the number of operations of the VSC [31].

The proposed methodology is assessed and compared to two controllers. The first is a conventional PI controller, which is the most common controller used in VSC. The second is an interconnection and damping assignment passivity-based control (IDA-PBC). IDA-PBC is suitable for managing PV plants because the VSC remains passive in the open loop and presents a port-Hamiltonian structure. IDA-PBC employs these properties to design a closed-loop controller and thereby preserves the passivity properties and guarantees a stable operation in the sense of Lyapunov. The controller gains are tuned using a metaheuristic technique called interactive teaching-learning optimizer, as performed by [32]. The impact of the proposed methodology is analyzed in four scenarios with penetration levels of 10%, 30%, 50%, and 80%. In addition, a decrease in the inertia of the synchronous machines from 100 to 25% is analyzed.

This paper is organized as follows: Section 2 explains the proposed methodology; Section 3 presents the dynamical model of the PV plant; Section 4 presents the proposed control and the design of the controller; Section 5 describes the test system and the proposed scenarios; the following Section 6 analyzes the main results; and Section 7 presents the conclusions of the study, outlines future research, and provides a reference list.

2. Proposed Methodology

The proposed methodology for improving POD in a power system with a high level of PV penetration is based on primary frequency and voltage control. This methodology

addresses the VSC of the PV plants. Here, the reference values are determined using the aforementioned concepts. Thus, the VSC is not constrained to behaving as a virtual synchronous generator. Primary frequency control is used to compensate for the POD, which adds a feedback signal to the $v_{dc}^{\star}$ (note that $\star$ denotes the desired reference value) of the DC-link to enhance system damping. Furthermore, the proposed methodology provides frequency support to the AC system by using a relation between the DC voltage and the angular frequency. To provide oscillation damping and frequency support, the PV systems can adjust the output power by adjusting the DC reference voltage. The swing equation relates the unbalanced power of an AC grid (which results in frequency deviation) as follows [33]:

$$2M\frac{\Delta\omega}{dt} = P_m - P_e - D_p(\omega - \omega^*), \tag{1}$$

where ω is the angular speed rotor, and ω^* is its setpoint, while $\Delta\omega$ is the deviation of the angular speed rotor. M is the inertia moment, P_m is the mechanical power, P_e is the electrical power, and D_p is a damping factor.

The mismatch between P_m and P_e caused by a varying load demand or disturbance in the primary motor may alter the rotor speed. The kinetic energy stored in the rotor could partially offset the unbalance power.

Similarly, the rate of stored energy in the DC-link of a VSC partially compensates the unbalance power. This could be explained by the following Equation [34]:

$$Cv_{dc}\frac{dv_{dc}}{dt} = P_{dc} - P_{VSC}, \tag{2}$$

where v_{dc} is the DC-link voltage, P_{dc} is the power generated by the PV cells, P_{VSC} is the power delivered to the power system by the VSC, and C is the DC-link capacitance.

From Figure 1, a relationship between the angular frequency and the DC voltage can be obtained by equating the shaft energy of a synchronous machine with the capacitor energy as follows:

$$2M\frac{d\omega}{dt} = Cv_{dc}\frac{dv_{dc}}{dt}. \tag{3}$$

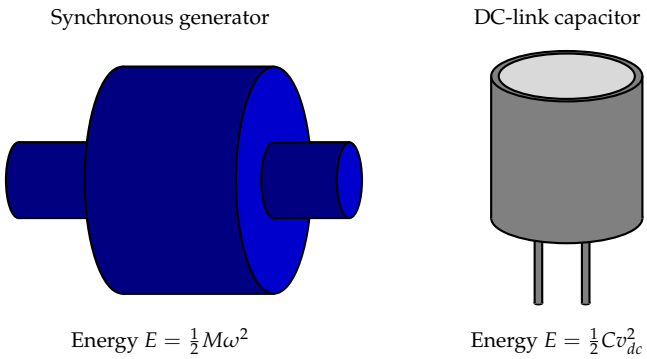

Figure 1. Analogy between the energies of the synchronous generator and the DC-link capacitor.

By integrating both the sides of Equation (3) and linearizing it, the following is obtained:

$$\Delta v_{dc} = \frac{2M}{Cv_{dc}^{\star}}\Delta\omega = K_{\omega}\Delta\omega, \tag{4}$$

where K_{ω} is the primary frequency gain.

A limitation of the proposed methodology corresponding to the primary frequency gain K_{ω}, which is due to the fact that its value directly depends on the desired virtual inertia

and the capacitor size of the DC-link. Therefore, it is not possible to assign an arbitrary primary gain without affecting the size of the DC-link capacitor.

It is important to mention that $v^{\star}_{dc}$ is defined as the sum of the nominal voltage of the DC-link and the error between the frequency signal ω and a reference value ($\omega^{\star}$) multiplied by a positive gain (K_{ω}). In addition, a deadband is considered to filter the noise in the frequency signal and thereby reduce the number of VSC operations. This increases the device's useful life [31]. The proposed methodology is illustrated in Figure 2.

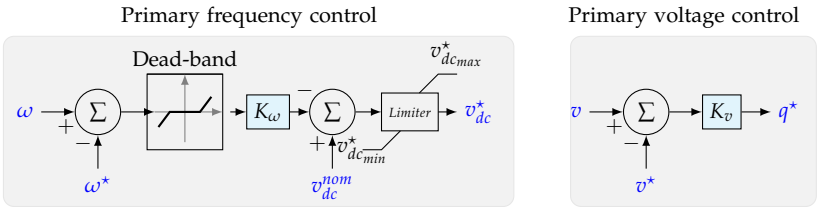

Figure 2. Reference values for the VSC.

Primary voltage control aids in regulating the voltage of the connected PV system. This consists of controlling the consumed/delivered reactive power q of the VSC. Here, $q^{\star}$ is defined as the reactive power desired plus the error between the voltage signal v at the connection point of the PV plant and its reference value ($q^{\star}$) multiplied by a positive gain (K_v) (see Figure 2).

Concurrently, the proposed methodology also considers the limitations of the active and reactive power transference of the VSC. This limitation is typically bounded by an over-current limiter. Figure 3 portrays the case where active power is prioritized over reactive power. This priority is selected because the objective of this study is to reduce the POD. This strategy limits $i^{\star}_{d}$ to the maximum current capacity $\pm i_{max}$, and it limits $i^{\star}_{q}$ so that it does not exceed the maximum current rating, which is expressed as follows [31]:

$$\begin{aligned} i_{d_{lim}} &\leq i_{max}, \\ -\sqrt{i^2_{max} - i^2_{d_{lim}}} \leq i_{q_{lim}} &\leq \sqrt{i^2_{max} - i^2_{d_{lim}}}, \end{aligned} \tag{5}$$

where i_{dq} are the currents flowing to the VSC, and i_{max} is the maximum current that can be supported by the VSC.

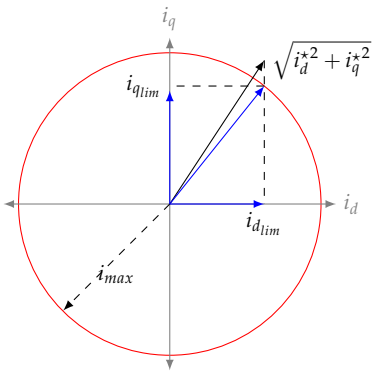

Figure 3. Priority given to $i_{d_{lim}}$ according to the current limiting strategy.

It should be mentioned that the proposed methodology is local and does not require any action in other parts of the system. In addition, there is no need to coordinate its operation with that of the other VSCs or existing power system stabilizers (PSSs). This operation mode is permanent and depends on the selected deadband. A deadband of 0.0005 pu is assumed, which is 30 mHz for the Colombian power system.

3. Photovoltaic Power Plants

Large PV plants are composed of hundreds of PV arrays connected to the power system via power inverters and step-up transformers. PV arrays convert solar energy into an electron flow by using the PV effect. This DC electricity is then converted to electric power by means of power electronics. PV plants are connected to power systems through VSCs. VSCs employ self-commutated switching, which can be gate turn-off thyristors (GTOs) or insulated gate bipolar transistors (IGBTs) [35]. These switches can be turned on or off in a controlled manner. In addition, the VSCs operate at a high switching frequency by utilizing the pulse-width modulation (PWM) technique.

Figure 4 illustrates the PV system employed in this study. It only shows the typical configuration of a VSC because it assumes a constant DC-link current. This assumption is valid because the solar radiation is considered to be constant for transient stability studies [27]. Therefore, none of the dynamics that existed before the DC-link are considered.

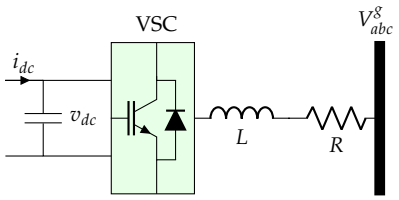

Figure 4. Typical interconnection of a PV plant through a VSC.

The average value model has been used for VSC dynamics in transient stability studies, as it omits the fast switching of converters [36]. This model is employed in this study.

Dynamic Model of a VSC

The dynamic model of the VSC in the dq reference frame is given by [37]:

$$\begin{aligned} L\dot{i}_d &= -R_T i_d - \omega L i_q + v_{dc} m_d - v_d, \\ L\dot{i}_q &= -R_T i_q + \omega L i_d + v_{dc} m_q - v_q, \\ C\dot{v}_{dc} &= i_s - i_d m_d - i_q m_q, \end{aligned} \tag{6}$$

where i_{dq} are the currents flowing to the transformer, and L and R_T are their inductance and resistive effects, respectively. The $m_{dq} \in [-1, 1]$ are the modulation indices of the VSC, the v_{dq} are the AC voltages in the main grid, and v_{dc} is the voltage of the DC-link. C is the DC-link capacitance of the VSC, and i_s represents the current delivered to the PV system, which is always positive ($i_s > 0$ for all PV plants). ω denotes the electrical grid's angular frequency, which is obtained as in a conventional phase-locked loop (PLL) system.

4. IDA-PBC Method

Interconnection and damping passivity-based control (IDA-PBC) theory is a robust and mathematically well-supported control theory for non-linear systems with Hamiltonian structures [38]. In general, IDA-PBC uses the open-loop Hamiltonian structure of a system to propose a closed-loop structure that preserves the passivity properties in order to design a controller that guarantees operational stability in the sense of Lyapunov [1].

4.1. Open-Loop Structure

A conventional structure of a port-Hamiltonian (pH) system for power electronic converters can be defined as expressed below:

Definition 1. *A port-Hamiltonian system for any power electronic converter under the averaging model can be expressed as [37]:*

$$\mathcal{D}\dot{x} = [\mathcal{J}(u) - \mathcal{R}]x + \varphi, \tag{7}$$

where $\mathcal{D} \in \mathbb{R}^{n\times n}$ is known as the inertia matrix, which is due to its similarities with models of mechanical systems. It is positive definite, so that $\mathcal{D} = \mathcal{D}^{\top}$. $\mathcal{J}(u) \in \mathbb{R}^{n\times n}$ corresponds to a skew-symmetric control matrix, which implies that $\mathcal{J}(u) = -\mathcal{J}^{\top}(u)$. $\mathcal{R} \in \mathbb{R}^{n\times n}$ is a positive semi-definite matrix that contains all the dissipative effects of the system. $\varphi \in \mathbb{R}^{n}$ corresponds to a vector that contains all the external inputs. $x \in \mathbb{R}^{n}$ represents all the state variables, and $u \in \mathbb{R}^{m}$ are the control inputs of the system. Note that, for under-actuated dynamical systems, $m \leq n$.

It is important to highlight that pH systems have the following characteristics [39]:

- *They are composed of two matrices that contain information on the interconnection between state variables and the energy dissipation properties of the system.*
- *They have an open-loop passive structure that can be utilized in a closed-loop design via passivity-based control theory.*
- *They are generally non-linear mathematical formulations that represent dynamical systems which can be derived from the Euler-Lagrange equations.*

The following mathematical relations can be established by comparing the dynamic system (7) with the dynamic model of the VSC [40]:

$$\begin{gathered}\mathcal{D} = \begin{bmatrix} L & 0 & 0 \\ 0 & L & 0 \\ 0 & 0 & C \end{bmatrix}, \quad \mathcal{J}(u) = \begin{bmatrix} 0 & -\omega L & m_d \\ \omega L & 0 & m_q \\ -m_d & -m_q & 0 \end{bmatrix}, \\ \mathcal{R} = \begin{bmatrix} R_T & 0 & 0 \\ 0 & R_T & 0 \\ 0 & 0 & 0 \end{bmatrix}, \quad x = \begin{pmatrix} i_d \\ i_q \\ v_{dc} \end{pmatrix}, \quad \varphi = \begin{pmatrix} -v_d \\ -v_q \\ i_s \end{pmatrix}.\end{gathered} \tag{8}$$

4.2. Desired Closed-Loop Structure

The open-loop dynamic system given in Equation (7) with the parameters presented in Equation (8) can be compared to the desired closed-loop dynamic system in order to design a controller using the passivation theory [41]. The desired closed-loop dynamics correspond to a stable bilinear dynamic system with modified interconnection and damping matrices. The general definition of a desired dynamic system for power electronic converters can be expressed as follows [41]:

Definition 2. *The desired closed-loop dynamic system for a VSC is formulated as*

$$\mathcal{D}\dot{\tilde{x}} = [\mathcal{J}^{\star}(u) - \mathcal{R}^{\star}]\tilde{x}, \tag{9}$$

where $\mathcal{J}^{\star}(u)$ and $\mathcal{R}^{\star}$ represent the desired interconnection and damping matrices that display characteristics identical to those of the open-loop dynamic system, i.e., they are skew-symmetric and positive semi-definite, respectively. In addition, $\tilde{x} = x - x^{\star}$, where $x^{\star}$ represents the desired operating point [41].

An important aspect in the modeling of a VSC under Park's reference frame is that $x^{\star}$ does not depend on time. This implies that $\dot{\tilde{x}} = \dot{x}$.

4.3. Controller Design

Note that it is now possible to compare the open-loop dynamic system (7) with the desired closed-loop one given by Equation (9). This yields [41]

$$\mathcal{J}^{\star}(u)x^{\star} = \mathcal{R}x - \mathcal{R}^{\star}\tilde{x} - \varphi. \tag{10}$$

Observe that the following is selected as the desired interconnection and damping matrices in order to obtain Equation (10) [1]:

$$\mathcal{J}^{\star}(u) = \mathcal{J}(u), \quad \mathcal{R}^{\star} = \begin{bmatrix} R_1 & 0 & 0 \\ 0 & R_2 & 0 \\ 0 & 0 & R_3 \end{bmatrix}. \tag{11}$$

The first two equations of (10) are solved to obtain the control laws m_d and m_q. This yields

$$\begin{aligned} m_d &= \left(v_{dc}^{\star}\right)^{-1}\Big(R_L i_d + \omega L i_q^{\star} + R_1\left(i_d^{\star} - i_d\right) + v_d\Big), \\ m_q &= \left(v_{dc}^{\star}\right)^{-1}\Big(R_L i_q - \omega L i_d^{\star} + R_2\Big(i_q^{\star} - i_q\Big) + v_q\Big). \end{aligned} \tag{12}$$

From Equation (12), it can be observed that the control input m_d can be used to control the current i_d, which is associated with the active power that is transferred from the PV plant to the power system. Meanwhile, m_q may be used to control the reactive power interchange between the VSC and power system [37]. Furthermore, the active power is directly related to the state of charge of the DC capacitor. This implies that only the power originating from the PV modules can be transferred to the power system, i.e., by using the current i_s. Hence, by solving the last equation of (12), the desired reference for the i_d current is obtained as a function of the desired voltage across the DC capacitor [37].

$$i_d^{\star} = m_d^{-1}\Big(i_s - m_q i_q^{\star} - R_3(v_{dc}^{\star} - v_{dc})\Big), \tag{13}$$

$$i_q^{\star} = \frac{q^{\star}}{v_d}. \tag{14}$$

4.4. Stability Test of the Controller

The main advantage of incorporating IDA-PBC in design control strategies for power electronic converters is the feasibility of ensuring stability in the sense of Lyapunov. Therefore, a candidate Lyapunov function $\mathcal{V}(\tilde{x})$ can be defined as follows:

$$\mathcal{V}(\tilde{x}) = \frac{1}{2}\tilde{x}^{\top}\mathcal{D}\tilde{x}. \tag{15}$$

Note that $\mathcal{V}(\tilde{x}) > 0\ \forall x \neq x^{\star}$ and $\mathcal{V}(0) = 0$. This clearly fulfills the first two conditions of the Lyapunov stability theorem [42].

The following is obtained by taking the temporal derivative of Equation (15), substituting Equation (9), and rearranging a few terms:

$$\begin{aligned} \dot{\mathcal{V}}(\tilde{x}) &= \tilde{x}^{\top}\mathcal{D}\dot{\tilde{x}} = \tilde{x}^{\top}[\mathcal{J}^{\star}(u) - \mathcal{R}^{\star}]\tilde{x} \\ &= \tilde{x}^{\top}\mathcal{J}^{\star}(u)\tilde{x} - \tilde{x}^{\top}\mathcal{R}^{\star}\tilde{x} = -\tilde{x}^{\top}\mathcal{R}^{\star}\tilde{x} < 0. \end{aligned} \tag{16}$$

It is important to highlight that Equation (16) allows guaranteeing the global asymptotic convergence of any IDA-PBC controllers applied to the VSC. Detailed proof of this is available in [37]. Finally, Figure 5 depicts the proposed control scheme and the application of the proposed methodology.

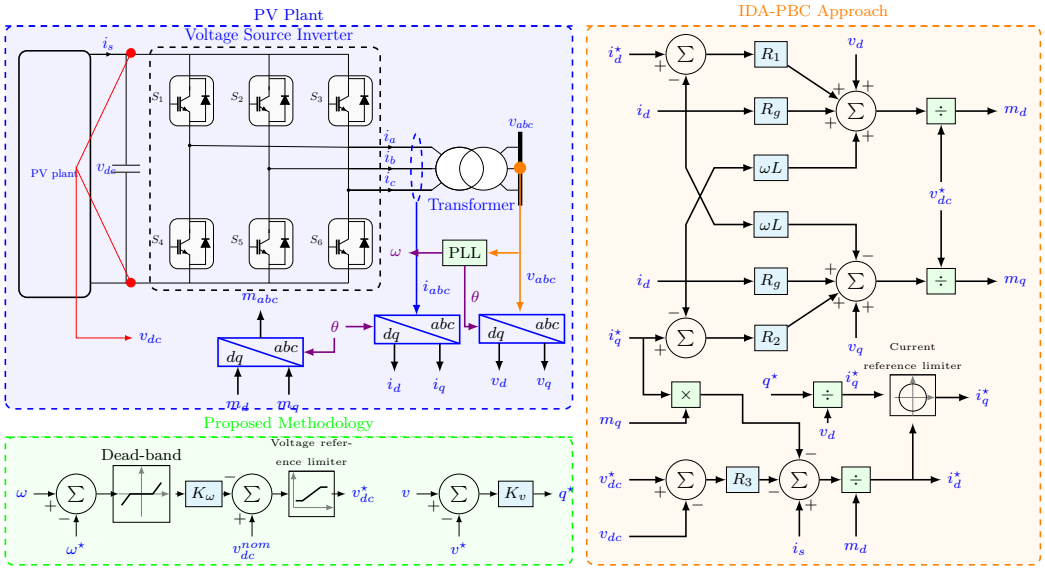

Figure 5. Proposed controller and methodological schemes.

5. Test System and Simulation Cases

5.1. Test System

Figure 6 depicts the 12-bus test system with different penetration levels of PV plants. This test system was proposed in [27], and it is used to demonstrate the effectiveness of the proposed methodology. The test system has four synchronous generators, six two-winding transformers, six loads, and eight transmission lines. The synchronous generators are equipped with AVR, PSS, and turbine governors. All the parameters of the test system are provided in [43]. Each PV plant employs the parameters listed in Table 1. In addition, the proposed methodology is assessed and compared to two controllers, such as a conventional PI controller and the IDA-PBC method. All the parameters are presented in Table 1.

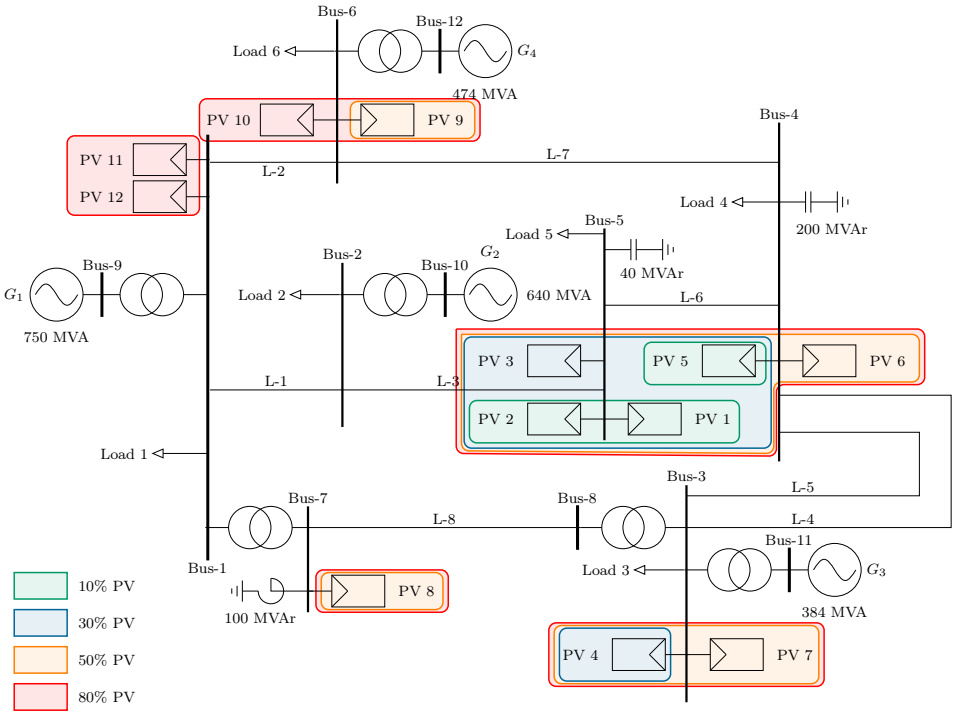

Figure 6. 12-bus test system with different penetration levels of PV plants.

Table 1. Data and parameter values.

Description	Parameter	Value	Description	Parameter	Value
PV system			IDA-PBC		
Nominal power	P_{nom}	0.5	Damping gain	R_1	0.8
Primary frequency control	K_ω	30	Damping gain	R_2	0.8
Primary voltage control	K_v	2	Damping gain	R_3	0.5
VSC			Outer Control		
DC-link capacitance	C	0.1	Proportional gain	K_p	2
Transformer inductance	L	0.15	Integral gain	K_i	0.5
Transformer resistance	R_T	0.015			
Maximum DC-link voltage	v_{dc}^{max}	1.2	*Inner control*		
Minimum DC-link voltage	v_{dc}^{min}	0.8	Proportional gain	K_p	25
Current limits	i^{max}	1.1	Integral gain	K_i	1.5

All parameters are per unit $S_{Base} = 100$ MW, $V_{Base} = 230$ kV.

It is important to mention that the controller gains are tuned using a metaheuristic technique called interactive teaching-learning optimizer, as performed in [32].

5.2. Simulation Cases

The following simulation cases are considered in order to demonstrate the effectiveness of the proposed methodology:

- *First case*: generator 4 is assumed to be disconnected abruptly.
- *Second case*: a short circuit on bus 8 for a period of 140 ms is considered.
- *Third case*: a permanent short circuit three-phase to the ground in the middle of line L-2 is considered. It is also supposed that the protection system operates at 140 ms.
- *Fourth case*: a load (equivalent to load 5) is considered to be connected abruptly at bus 5.

Four scenarios with different penetration levels are also considered in order to analyze the impact of the PV plants in the power system. The PV plant penetration level is gradually increased across the considered scenarios to illustrate the evolution of the power systems. The penetration level and the number of PV plants and their locations are presented in Figure 6.

- Scenario 1: three PV plants with a 10% penetration level are considered. These represent the current power systems that incorporate renewable energy.
- Scenario 2: five PV plants with a penetration level of 30% are assumed in this scenario. These represent an eventual power system with renewable energy inclusion in the short term.
- Scenario 3: nine PV plants with a 50% penetration level are considered. This denotes a feasible situation with a penetration that exceeds the current limits of renewable inclusion.
- Scenario 4: twelve PV plants with an 80% penetration level are considered.

Note that the active power produced by the PV plants in all the scenarios is assumed to be equal. The operating conditions of the synchronous generators for the four scenarios are listed in Table 2.

Table 2. Operating conditions of the synchronous generators.

	Generator							
	G1		G2		G3		G4	
	P	V	P	V	P	V	P	V
Scenario 1	3.42	1.00	4.00	1.01	2.70	1.01	3.30	1.01
Scenario 2	2.53	1.00	3.27	1.01	1.97	1.01	2.57	1.01
Scenario 3	1.82	1.00	2.55	1.01	1.25	1.01	1.85	1.01
Scenario 4	0.7	1.00	0.8	1.01	0.8	1.01	0.65	1.01

All the parameters are per unit. $S_{Base} = 100$ MW, $V_{Base} = 230$ kV.

For all cases, it is assumed that the perturbation occurs at 1.0 s. Furthermore, it is considered that the proposed methodology is implemented with the IDA-PBC as presented in Section 4, whereas the conventional converter controller (PI) does not include the proposed methodology.

6. Results

The four cases and the 12-bus test system with different penetration levels of PV plants (see Figure 6) were implemented in MATLAB/Simulink (MATLAB2019b) and run on a desk computer (with an INTEL(R) Core(TM) i7-7700 CPU @ 3.60 GHz, 8 GB RAM, and 64-bit Windows 10 Professional).

6.1. First Case

This case shows the capability of the proposed methodology to compensate for the POD when generator 4 becomes disconnected. This generator produces 22.75, 17.75, 12.75, and 4.48% of the total active power in the test system for scenarios 1, 2, 3, and 4, respectively. In each scenario, the active power produced is distributed equally among the other three generators after generator 4 is disconnected.

The dynamic responses of the rotor speed deviations of synchronous generator 3, the terminal voltage of generator 1, and the active power of PV plant 1 are illustrated in Figure 7.

Note that $\Delta\omega_3$ helps determine the extent to which the frequency of the test system is affected (see Figure 7a). Scenario 1 exhibits the largest decrease in $\Delta\omega_3$. This occurs because the disconnection of generator 4 when the PV penetration is 10% produces a greater power imbalance. This is because 22.75% of the total generation disappears abruptly, unlike the other three scenarios, where the contribution of generator 4 is lower.

Figure 7a also shows that the proposed methodology enables the mitigation of POD, thereby enhancing the power system's stability without constraining the VSC to emulate the dynamics of a synchronous generator.

Figure 7b shows that the voltage profiles stabilize faster when primary voltage control is employed. This confirms that the VSC of a PV plant can be used to improve its voltage profile under large disturbances.This occurs on the generator 1 bus and on all the other buses in the power system.

The active power produced by PV plant 1 shows greater changes when primary frequency control is implemented (see Figure 7c). These shifts are necessary to compensate for the POD in the power system, so that less time is required for the frequency oscillations to decrease (Figure 7a). In scenario 1, it is also evident that the active power produced shows a greater shift in comparison with scenarios 2, 3, and 4. This is because scenario 1 has fewer PV plants that may produce a power imbalance in the power system. In the design of PV plants, it is necessary to examine whether the VSCs can safely support these overloads and thereby ascertain whether the PV plants can produce the required active power.

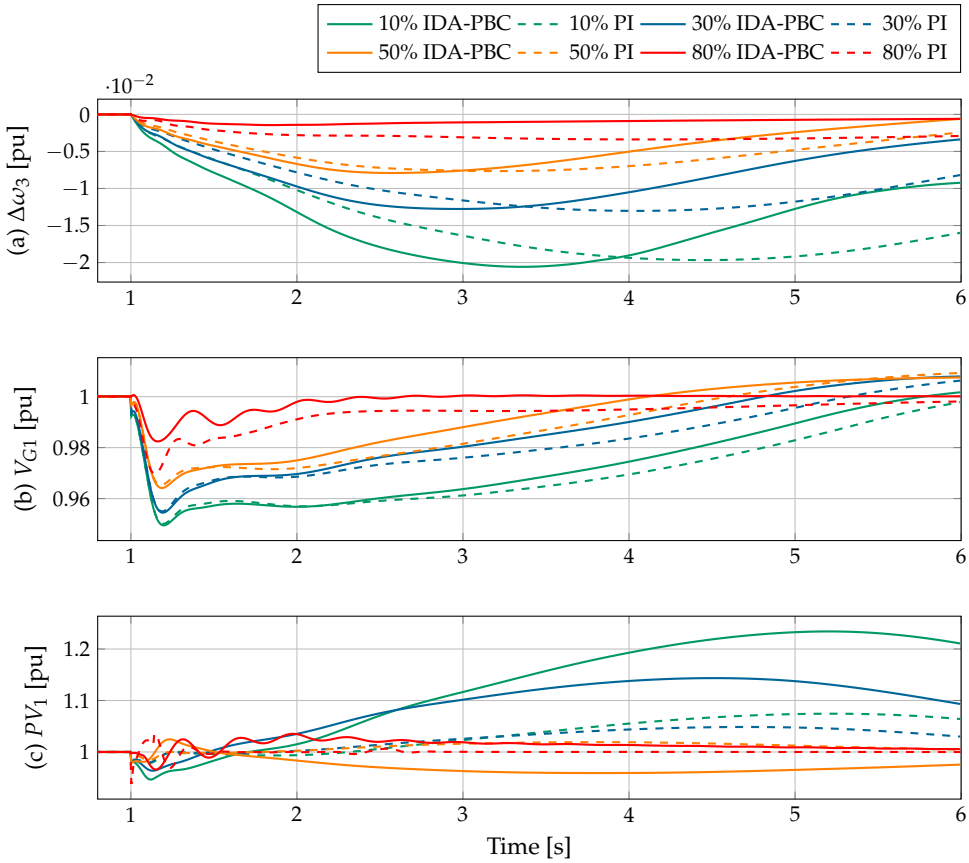

Figure 7. Response of the test system to the abrupt disconnection of generator 4: (**a**) rotor speed deviation of generator 3, (**b**) terminal voltage of generator 1, and (**c**) active power of PV plant 1.

6.2. Second Case

This case involves analyzing the effect of a large-scale disturbance in the power system, which is evidenced by a short circuit event on bus 8. Figure 8 presents the rotor speed deviation of generator 3, the voltage profile at the terminals of generator 1, the active power provided by PV plant 1, and the active power of generator 2. Figure 8a shows the direct relationship between the PV penetration level and the frequency deviation: higher frequency oscillations are evidenced when the active power generation is minimal. The frequency deviations are minimal when the active power of the PV system is maximal. This behavior is to be expected because the capability to reduce frequency deviation is associated with the current capabilities of the PV system, as well as with the primary control depicted in Figure 2.

Note that the application of the proposed methodology with the IDA-PBC approach reduces the frequency deviations from those of the PI approach in the four PV penetration scenarios. The frequency oscillations for scenarios 1, 2, 3, and 4 decrease in comparison with the maximum value obtained without using the proposed methodology, i.e., by 16.8%, 38.43%, 37.53%, and 76.94%, respectively. This demonstrates that the proposed methodology's effect on the damping of the frequency oscillations benefits the synchronous machines and reduces the stress on the shaft.

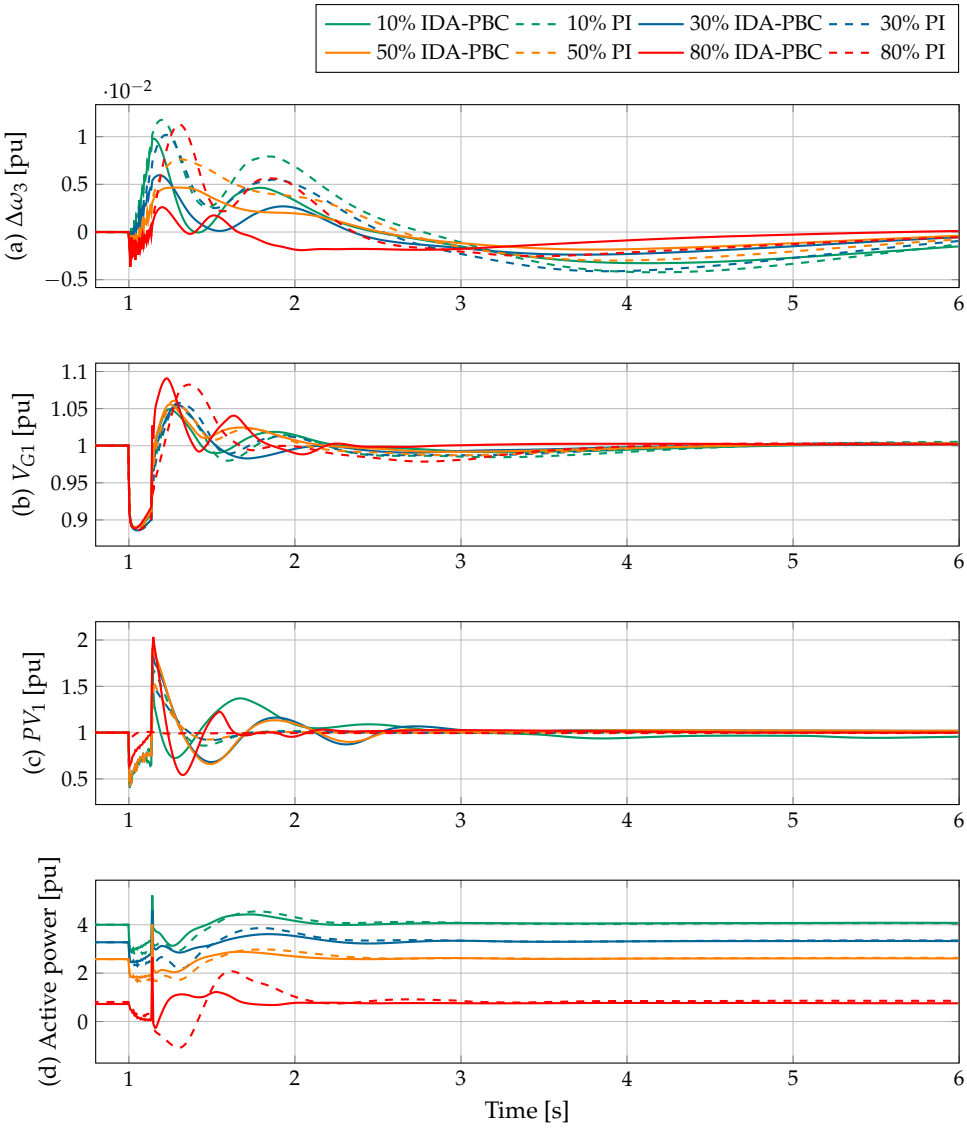

Figure 8. Response of the test system to a short circuit on bus 8 for 140 ms: (**a**) rotor speed deviation of generator 3, (**b**) terminal voltage of generator 1, (**c**) active power of PV plant 1, and (**d**) active power of generator 2.

Figure 8b shows the dynamic performance of the voltage profile at the terminals of generator 1. Here, the oscillations in the voltage profile are higher for the PI approach in all the cases than for the proposed IDA-PBC control methodology. Nevertheless, the system recovers its normal behavior for both control strategies 4 s after the fault has been clarified. This behavior shows that the PI and IDA-PBC approaches allow maintaining the power system's stability during dramatic short-circuit events by considering a wide range of variations regarding PV power penetration.

Figure 8c depicts the active power output of PV plant 1. Note that, unlike the behavior depicted in Figure 8a,b, the IDA-PBC approach shows higher oscillations in the active power output than PI. This is to be expected, given that the proposed primary voltage and frequency control operates as a function of the active power provided by the PV plant. This implies that higher active power variations are required to reduce frequency (voltage) oscillations in the least possible time.

Figure 8d shows that the active power oscillations of generator 2 are lower when the proposed methodology is employed. In addition, for all the penetration levels, the proposed methodology has a faster response and stabilizes the system in less time.

6.3. Third Case

This case simulates the proposed methodology's contribution to improving the power system's stability when a topology shift occurs together with the tripping of the transmission line L-2. Figure 9 shows the dynamic performance of the rotor speed deviation, as well as the voltage profile in generator 3, the power output in PV plant 1, and the active power of generator 2.

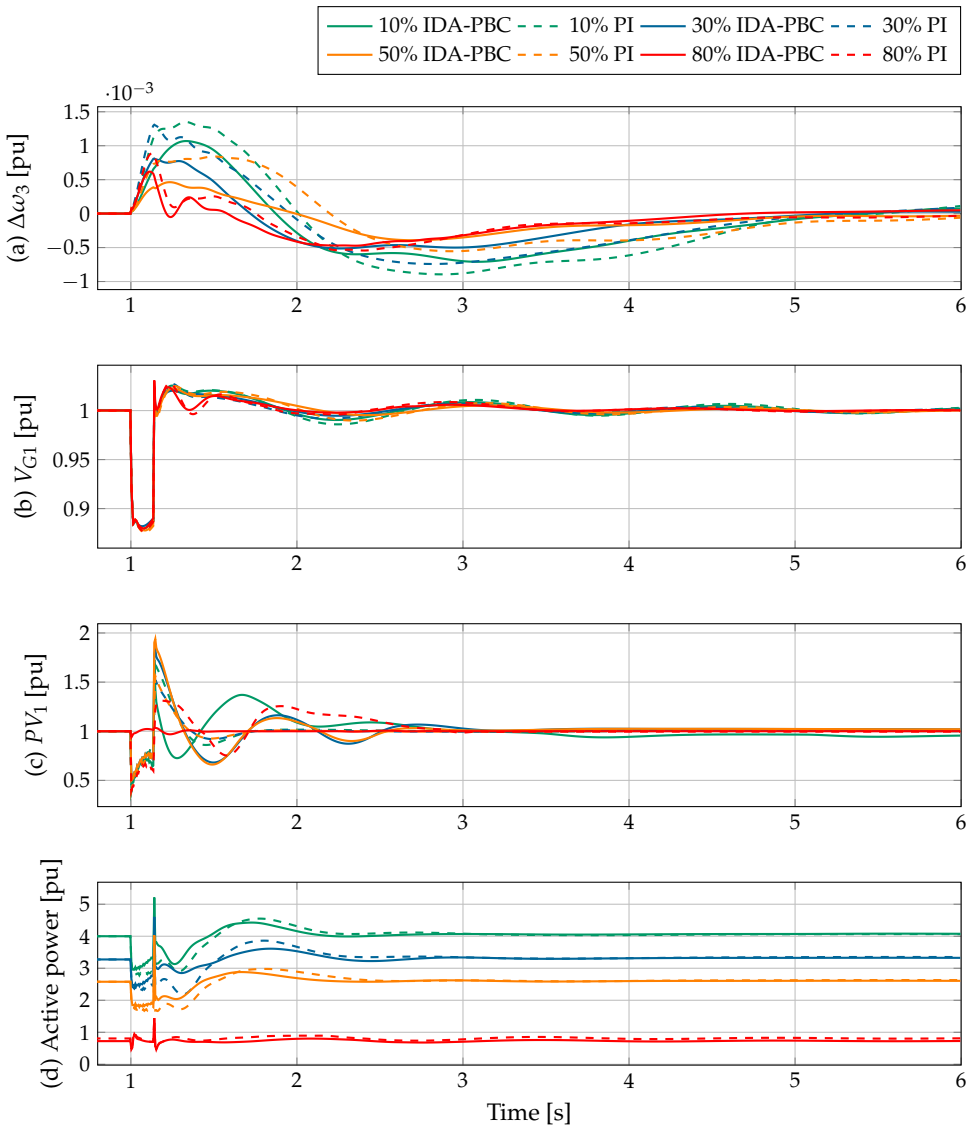

Figure 9. Response of the test system to a short circuit in the middle of line L-2: (**a**) rotor speed of generator 3, (**b**) terminal voltage of generator 1, (**c**) active power of PV plant 1, and (**d**) active power of generator 2.

Note that the PI control exhibits higher oscillations in the frequency and voltage signals (see Figure 9a,b) than the proposed IDA-PBC methodology. In addition, the active power outputs of PV plant 1 and generator 2 have a similar interpretation to that of the previous case (see Figure 9c,d). Finally, note that this case illustrates the advantage of controlling PV plants in power grids via the primary control approach, i.e., the transient conditions after large-scale disturbances, including topological grid variations, can be significantly improved in comparison with conventional approaches.

6.4. Fourth case

This case investigates the capability of the proposed methodology to alleviate POD when a load is connected abruptly at bus 5. Figure 10 illustrates the rotor speed deviation of generator 3, the voltage profile at the terminals of generator 1, and the active power delivered by PV plant 1. As previously indicated, the dynamic response is better when the proposed methodology is used. In addition, the proposed approach stabilizes the system faster, even in light of an abrupt connection.

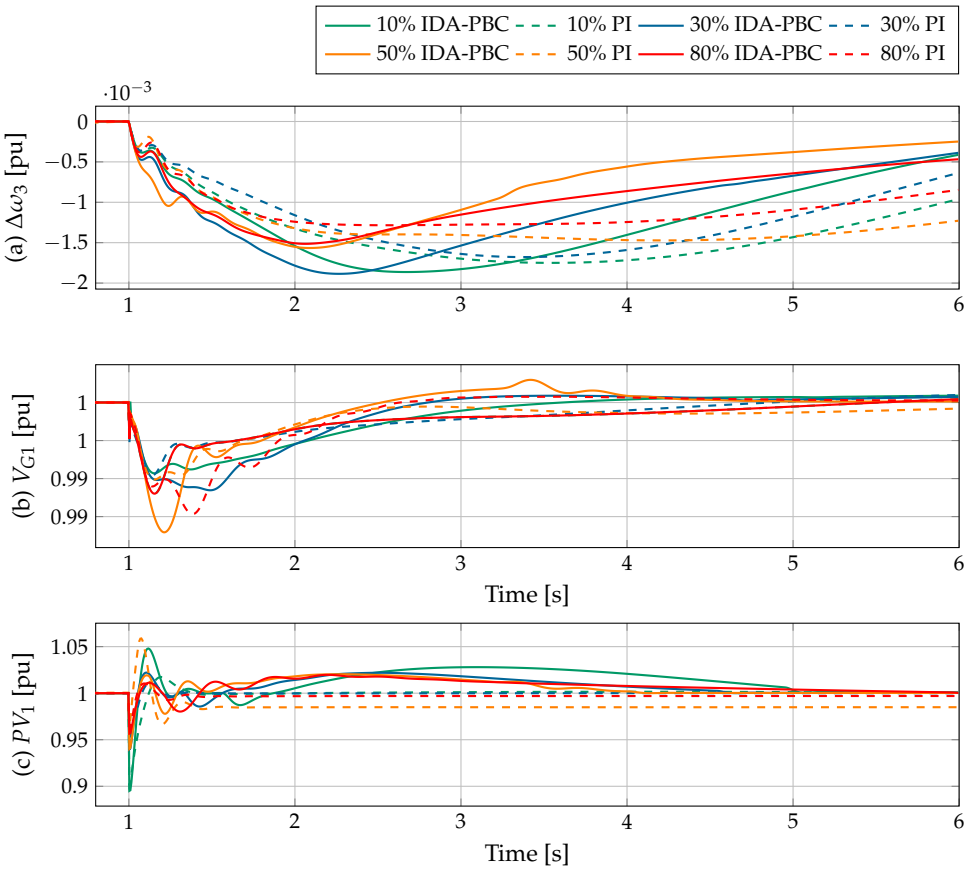

Figure 10. Response of the test system to the abrupt connection of a load at bus 5: (**a**) rotor speed of generator 3, (**b**) terminal voltage of Generator 1, and (**c**) active power of PV plant 1.

It is important to note that the primary frequency control serves as additional inertia for the power system; it contributes decisively to dampening the variation rate in the frequency and, thereby, its maximum deviation. This can be verified by comparing $\Delta\omega$ when the primary frequency control is implemented and when it is not in all the scenarios (see Figures 7a–10a). In addition, the decrease in the frequency deviation becomes evident in light of an increased penetration of PV systems.

It can be observed that the active power of the PV system increases dramatically when the large disturbance disappears (e.g., a short circuit) for approximately 1.4 s (see Figures 7c–10c). This occurs because the RMS voltage in all the system nodes increases dramatically after the large disturbance event, thus increasing the instantaneous active power in the entire power system.

6.5. Analysis of the Decrease in Inertia

This subsection examines the capability of the proposed methodology to enhance stability when the synchronous machine's inertia is reduced from 100 to 25%. This analysis is carried out under the conditions of the second case because it displays the largest angular

frequency oscillation. Figure 11 illustrates the maximum average frequency deviation of the synchronous machines when a reduction in their inertia is considered.

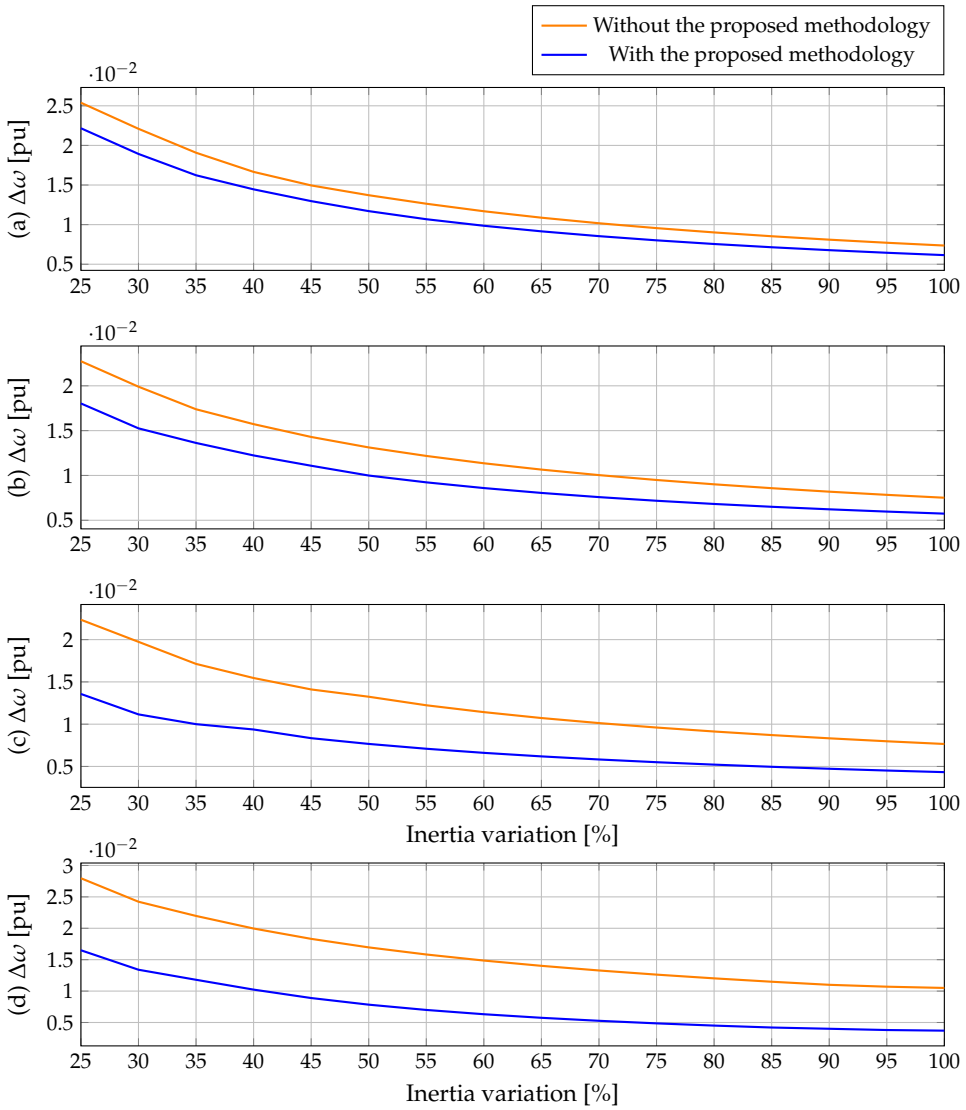

Figure 11. Maximum average of $\Delta\omega$ when the inertia of the synchronous machines is reduced: (**a**) 10%, (**b**) 30%, (**c**) 50%, and (**d**) 80% penetration.

Figure 11 shows that the maximum average of $\Delta\omega$ is less when the proposed methodology is implemented. In addition, this maximum average of $\Delta\omega$ is reduced as the inertia of the synchronous machines decreases. Finally, it can also be observed that the maximum average of $\Delta\omega$ decreases as the penetration level of PV systems increases. This is because there are more PV systems that contribute inertia to the power system.

6.6. Complementary Analysis

Table 3 presents the integral of the time-weighted absolute error (ζ) for the rotor speed deviations and the generator terminal voltages. These are determined as follows:

$$\begin{aligned} \zeta_\omega &= \frac{1}{4}\sum_{k=1}^{4}\int_0^{t_{sim}} t'|\Delta\omega_k|dt', \\ \zeta_v &= \frac{1}{4}\sum_{k=1}^{4}\int_0^{t_{sim}} t'|\Delta V_{G_k}|dt'. \end{aligned} \tag{17}$$

Table 3. Integral of the time-weighted absolute error for rotor speed deviations and generator terminal voltages.

		First Case		Second Case		Third Case		Fourth Case	
		ζ_ω	ζ_v	ζ_ω	ζ_v	ζ_ω	ζ_v	ζ_ω	ζ_v
Scenario 1	PI	46.31	61.92	8.89	27.61	1.65	17.26	4.17	4.76
	PBC	42.68	56.04	7.09	15.55	0.92	14.63	3.36	4.36
Scenario 2	PI	27.31	36.27	6.72	19.21	0.75	11.01	3.65	4.53
	PBC	24.86	35.98	4.55	14.29	0.58	10.64	2.86	4.27
Scenario 3	PI	20.62	32.48	5.24	16.25	0.53	12.91	3.96	4.58
	PBC	12.01	31.59	3.78	15.89	0.42	10.06	1.92	3.68
Scenario 4	PI	8.97	15.05	5.39	23.33	0.78	9.69	3.26	4.23
	PBC	2.57	2.76	2.27	13.37	0.38	8.12	2.47	3.57

The results presented in Table 3 qualitatively demonstrate the enhanced performance of the proposed methodology. Virtual inertia is added to the power system by employing frequency control. In addition, ζ_ω decreases when the penetration level of the PV plants increases.

Figure 12 illustrates the computed voltage reference in the DC-link for PV plant 1, as shown in Figure 2, and their dynamical responses of IDA-PBC for scenario 4 (80% PV plants). It can be seen that the IDA-PBC approach can follow the reference generated by the proposed methodology with a good performance.

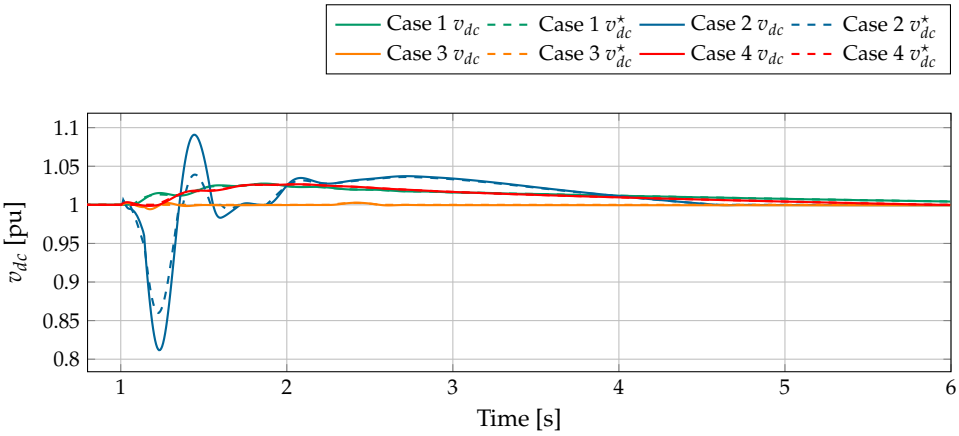

Figure 12. Response of the DC-link voltage for the cases.

7. Conclusions

In this study, a methodology based on primary voltage and frequency control was presented to improve the POD in a power system with high penetration levels of PV generation. The proposed methodology exhibited the advantage of enhancing the dynamic response of the power system without forcing the VSC to behave as a virtual synchronous generator. This is an advantage because no new dynamics are introduced in calculating the VSC reference values, which is required for a virtual synchronous generator. This methodology was developed by relating the energy stored in the VSC of the DC-link and the energy stored in the synchronous machine's shaft. In addition, the methodology considered the operating limits of the VSC, which, in turn, limits the injection of reactive power if these boundaries are exceeded.

Time-domain simulations were performed considering four penetration levels (10%, 30%, 50%, and 80%) of PV generation and four large disturbances in the test power system. The frequency oscillations were reduced to four penetration levels when the proposed methodology was implemented in the PV plants. The values of these reductions were 16.8%, 38.43%, 37.53%, and 76.94% in comparison with the case where the proposed methodology

was not implemented. These reductions in the frequency oscillations of the power system allowed reducing the stress on the synchronous machines and their shafts. In addition, it was observed that the oscillation of the DC-link voltages decreased. Hence, their stress and the effects on the capacitors were also reduced. The proposed methodology was also assessed with regard to a reduction in inertia in synchronous machines from 100 to 25%, where the frequency deviations were reduced when the proposed primary control was employed. Finally, it can be highlighted that the power system stability improved when the proposed methodology was equipped in the PV plants. Therefore, this methodology could play an essential role in the operation of power systems, controlling their voltage and frequency as well as improving the damping of the power and frequency oscillations when a large disturbance occurs.

Author Contributions: Conceptualization, methodology, software, and writing (review and editing): W.G.-G., O.D.M., A.M.-C., Á.M.-Q. and J.C.H. All authors have read and agreed to the published version of the manuscript.

Funding: This work was partially supported by the Center for Research and Scientific Development of Universidad Distrital Francisco José de Caldas, under grant 1643-12-2020 associated with the project *Desarrollo de una metodología de optimización para la gestión óptima de recursos energéticos distribuidos en redes de distribución de energía eléctrica* [Development of an optimization methodology for the optimal management of distributed energy resources in electrical energy distribution networks].

Data Availability Statement: No new data were created or analyzed in this study. Data sharing is not applicable to this article.

Conflicts of Interest: The authors declare no conflict of interest.

References

1. Gil-González, W.; Garces, A.; Fosso, O.B.; Escobar-Mejía, A. Passivity-based control of power systems considering hydro-turbine with surge tank. *IEEE Trans. Power Syst.* **2019**, *35*, 2002–2011. [CrossRef]
2. Ruiz, X. Role of the european union in the climate change negotiations. In *UNISCI Discussion Papers*; Taylor & Francis: London, UK; 2015; pp. 105–129.
3. Kabir, E.; Kumar, P.; Kumar, S.; Adelodun, A.A.; Kim, K.H. Solar energy: Potential and future prospects. *Renew. Sustain. Energy Rev.* **2018**, *82*, 894–900. [CrossRef]
4. Jäger-Waldau, A.; Kougias, I.; Taylor, N.; Thiel, C. How photovoltaics can contribute to GHG emission reductions of 55% in the EU by 2030. *Renew. Sustain. Energy Rev.* **2020**, *126*, 109836. [CrossRef]
5. Milano, F.; Manjavacas, A.O. *Frequency Variations in Power Systems: Modeling, State Estimation, and Control*; John Wiley & Sons: Hoboken, NJ, USA, 2020.
6. Eftekharnejad, S.; Vittal, V.; Heydt, G.T.; Keel, B.; Loehr, J. Impact of increased penetration of photovoltaic generation on power systems. *IEEE Trans. Power Syst.* **2013**, *28*, 893–901. [CrossRef]
7. Eftekharnejad, S.; Vittal, V.; Heydt, G.T.; Keel, B.; Loehr, J. Small signal stability assessment of power systems with increased penetration of photovoltaic generation: A case study. *IEEE Trans. Sustain. Energy* **2013**, *4*, 960–967. [CrossRef]
8. Harnefors, L.; Yepes, A.G.; Vidal, A.; Doval-Gandoy, J. Passivity-Based Controller Design of Grid-Connected VSCs for Prevention of Electrical Resonance Instability. *IEEE Trans. Ind. Electron.* **2015**, *62*, 702–710. [CrossRef]
9. Kazemi Golkhandan, R.; Aghaebrahimi, M.R.; Farshad, M. Control strategies for enhancing frequency stability by DFIGs in a power system with high percentage of wind power penetration. *Appl. Sci.* **2017**, *7*, 1140. [CrossRef]
10. Delille, G.; Francois, B.; Malarange, G. Dynamic frequency control support by energy storage to reduce the impact of wind and solar generation on isolated power system's inertia. *IEEE Trans. Sustain. Energy* **2012**, *3*, 931–939. [CrossRef]
11. Tamimi, B.; Cañizares, C.; Bhattacharya, K. System stability impact of large-scale and distributed solar photovoltaic generation: The case of Ontario, Canada. *IEEE Trans. Sustain. Energy* **2013**, *4*, 680–688. [CrossRef]
12. Wang, Y.; Silva, V.; Lopez-Botet-Zulueta, M. Impact of high penetration of variable renewable generation on frequency dynamics in the continental Europe interconnected system. *IET Renew. Power Gener.* **2016**, *10*, 10–16. [CrossRef]
13. Edrah, M.; Lo, K.L.; Anaya-Lara, O. Impacts of high penetration of DFIG wind turbines on rotor angle stability of power systems. *IEEE Trans. Sustain. Energy* **2015**, *6*, 759–766. [CrossRef]
14. Gevorgian, V.; Zhang, Y.; Ela, E. Investigating the impacts of wind generation participation in interconnection frequency response. *IEEE Trans. Sustain. Energy* **2014**, *6*, 1004–1012. [CrossRef]
15. Korai, A.; Erlich, I. Frequency dependent voltage control by DER units to improve power system frequency stability. In Proceedings of the 2015 IEEE Eindhoven PowerTech, Eindhoven, The Netherlands, 29 June–2 July 2015; pp. 1–6.

16. Silva-Saravia, H.D.; Pulgar, H.A.; Tolbert, L.M.; Schoenwald, D.A.; Ju, W. Enabling Utility-Scale Solar PV Plants for Electromechanical Oscillation Damping. *IEEE Trans. Sustain. Energy* **2020**, *12*, 138–147. [CrossRef]
17. Jamsheed, F.; Iqbal, S.J. An Adaptive Neural Network-Based Controller to Stabilize Power Oscillations in Wind-integrated Power Systems. *IFAC-PapersOnLine* **2022**, *55*, 740–745. [CrossRef]
18. Zenelis, I.; Wang, X. A model-free sparse wide-area damping controller for inter-area oscillations. *Int. J. Electr. Power Energy Syst.* **2022**, *136*, 107609. [CrossRef]
19. Alsakati, A.A.; Vaithilingam, C.A.; Naidu, K.; Rajendran, G.; Alnasseir, J.; Jagadeeshwaran, A. Particle Swarm Optimization for Tuning Power System Stabilizer towards Transient Stability Improvement in Power System Network. In Proceedings of the 2021 IEEE International Conference on Artificial Intelligence in Engineering and Technology (IICAIET), Kota Kinabalu, Malaysia, 13–15 September 2021; pp. 1–6.
20. Eladany, M.M.; Eldesouky, A.A.; Sallam, A.A. Power system transient stability: An algorithm for assessment and enhancement based on catastrophe theory and FACTS devices. *IEEE Access* **2018**, *6*, 26424–26437. [CrossRef]
21. Penchalaiah, G.; Ramya, R. Investigation on Power System Stability Improvement Using Facts Controllers. In *Proceedings of International Conference on Power Electronics and Renewable Energy Systems*; Springer: Singapore, 2022; pp. 499–506.
22. Naeem, A.; Atif, A. Transient Stability of Power System by Static VAR Compensator (SVC) and Power System Stabilizers (PSS) using MATLAB/Simulink. *SSRG Int. J. Electr. Electron. Eng. (SSRG-IJEEE)* **2018**, *5*, 16–20.
23. He, P.; Fang, Q.; Jin, H.; Ji, Y.; Gong, Z.; Dong, J. Coordinated design of PSS and STATCOM-POD based on the GA-PSO algorithm to improve the stability of wind-PV-thermal-bundled power system. *Int. J. Electr. Power Energy Syst.* **2022**, *141*, 108208. [CrossRef]
24. Suul, J.A.; D'Arco, S.; Guidi, G. Virtual synchronous machine-based control of a single-phase bi-directional battery charger for providing vehicle-to-grid services. *IEEE Trans. Ind. Appl.* **2016**, *52*, 3234–3244. [CrossRef]
25. Mo, O.; D'Arco, S.; Suul, J.A. Evaluation of virtual synchronous machines with dynamic or quasi-stationary machine models. *IEEE Trans. Ind. Electron.* **2017**, *64*, 5952–5962. [CrossRef]
26. Hou, X.; Sun, Y.; Zhang, X.; Lu, J.; Wang, P.; Guerrero, J.M. Improvement of frequency regulation in VSG-based AC microgrid via adaptive virtual inertia. *IEEE Trans. Power Electron.* **2020**, *35*, 1589–1602. [CrossRef]
27. Remon, D.; Cantarellas, A.M.; Mauricio, J.M.; Rodriguez, P. Power system stability analysis under increasing penetration of photovoltaic power plants with synchronous power controllers. *IET Renew. Power Gener.* **2017**, *11*, 733–741. [CrossRef]
28. Remon, D.; Cañizares, C.A.; Rodriguez, P. Impact of 100-MW-scale PV plants with synchronous power controllers on power system stability in northern Chile. *IET Gener. Transm. Dis.* **2017**, *11*, 2958–2964. [CrossRef]
29. Markovic, U.; Chu, Z.; Aristidou, P.; Hug, G. LQR-based adaptive virtual synchronous machine for power systems with high inverter penetration. *IEEE Trans. Sustain. Energy* **2018**, *10*, 1501–1512. [CrossRef]
30. Markovic, U.; Stanojev, O.; Aristidou, P.; Vrettos, E.; Callaway, D.; Hug, G. Understanding small-signal stability of low-inertia systems. *IEEE Trans. Power Syst.* **2021**, *36*, 3997–4017. [CrossRef]
31. Milano, F.; Manjavacas, Á.O. *Converter-Interfaced Energy Storage Systems: Context, Modelling and Dynamic Analysis*; Cambridge University Press: Cambridge, UK, 2019.
32. Gil-González, W.; Montoya, O.D.; Garces, A. Direct power control of electrical energy storage systems: A passivity-based PI approach. *Electr. Power Syst. Res.* **2019**, *175*, 105885. [CrossRef]
33. Machowski, J.; Lubosny, Z.; Bialek, J.W.; Bumby, J.R. *Power System Dynamics: Stability and Control*, 3rd ed.; John Wily & Sons: Hoboken, NJ, USA, 2020.
34. Ortega, A.; Milano, F. Generalized model of VSC-based energy storage systems for transient stability analysis. *IEEE Trans. Power Syst.* **2015**, *31*, 3369–3380. [CrossRef]
35. Bhatt, G.; Affljulla, S. Analysis of large scale PV penetration impact on IEEE 39-Bus power system. In Proceedings of the 2017 IEEE 58th International Scientific Conference on Power and Electrical Engineering of Riga Technical University (RTUCON), Riga, Latvia, 12–13 October 2017; pp. 1–6.
36. Montoya, O.D. Passivity-Based Analysis and Control of AC Microgrids: Integration, Operation and Control of Energy Storage Systems. Ph.D. Thesis, Universidad Tecnológica de Pereira, Pereira, Colombia, 2019.
37. Serra, F.M.; De Angelo, C.H. IDA-PBC controller design for grid connected Front End Converters under non-ideal grid conditions. *Electr. Power Syst. Res.* **2017**, *142*, 12–19. [CrossRef]
38. Gupta, Y.; Chatterjee, K.; Doolla, S. Controller design, analysis and testing of a three-phase VSI using IDA–PBC approach. *IET Power Electron.* **2020**, *13*, 346–355. [CrossRef]
39. Ortega, R.; van der Schaft, A.; Maschke, B.; Escobar, G. Interconnection and damping assignment passivity-based control of port-controlled Hamiltonian systems. *Automatica* **2002**, *38*, 585–596. [CrossRef]
40. Gil-González, W.; Serra, F.M.; Montoya, O.D.; Ramírez, C.A.; Orozco-Henao, C. Direct Power Compensation in AC Distribution Networks with SCES Systems via PI-PBC Approach. *Symmetry* **2020**, *12*, 666. [CrossRef]
41. Cisneros, R.; Pirro, M.; Bergna, G.; Ortega, R.; Ippoliti, G.; Molinas, M. Global tracking passivity-based PI control of bilinear systems: Application to the interleaved boost and modular multilevel converters. *Control Eng. Pract.* **2015**, *43*, 109–119. [CrossRef]
42. Perko, L. *Differential Equations and Dynamical Systems*; Springer Science & Business Media: Berlin/Heidelberg, Germany, 2013; Volume 7.
43. Gil-González, W. Passivity–Based Control and Stability Analysis for Hydro–Solar Power Systems. Ph.D. Thesis, Universidad Tecnológica de Pereira, Pereira, Colombia, 2019.